All-Optical Switching of Liquid Crystals at Terahertz Frequencies Enabled by Metamaterials

BENJAMIN BEDDOES,[1,*] ELENI PERIVOLARI,[2] MALGOSIA KACZMAREK,[1] VASILIS APOSTOLOPOULOS,[1] AND VASSILI A. FEDOTOV[3]

[1]*Physics and Astronomy, University of Southampton, Highfield, SO17 1BJ, UK*
[2]*EMPA Swiss Federal Laboratories for Material Science and Technology, Ueberlandstrasse 129, 8600 Dübendorf, Switzerland*
[3]*Optoelectronics Research Centre & Centre for Photonic Metamaterials, University of Southampton, Highfield, SO17 1BJ, UK*
[*]*B.Beddoes@soton.ac.uk*

Abstract:

Nematic liquid crystals integrated with metallic resonators (metamaterials) are intriguing hybrid systems, which not only offer added optical functionalities, but also promote strong light-matter interactions. In this report, we show with a simple analytical model that the electric field generated by a conventional oscillator-based terahertz time domain spectrometer is strong enough to induce partial, all-optical switching of nematic liquid crystals in such hybrid systems. Our analysis provides a robust theoretical footing for the mechanism of optical nonlinearity of liquid crystals, which was recently proposed to explain anomalous resonance frequency shift in liquid crystal-loaded terahertz metamaterials [1]. This method offers a systematic approach to explore nonlinearity within hybrid liquid crystal cells; paves the way towards increased efficiency of existing devices; and broadens the range of applications of liquid crystals in the terahertz frequency range. This method offers a combinatorial way to study molecular liquid crystal interactions in the bulk and explore the related optical nonlinearity through interfacing with resonant structures.

1. Introduction

Terahertz (THz) technologies have shown significant potential in several important application areas including: non-disruptive drugs sensing [2,3], security [4–6], medicine and life sciences [7] and next-generation short-range wireless systems operating at higher data transfer rates than currently available [8]. Yet, research in this field is still primarily focused on finding ways to both control and manipulate THz radiation effectively [9–12]. A particular focus is on the development of tuneable, compact and cheap devices such as modulators [13, 14] and phase shifters [15]. Liquid crystals (LCs) could offer a viable solution being already at the core of many technologies across most of the electromagnetic spectrum, such as: smart displays [16, 17], smart windows [18, 19], flat optics [20–23], and flexible electronics [24–26]. However, to operate efficiently in the THz spectral domain, LC-based optical components must be several hundred microns (or more) thick. This is due to the relatively low birefringence of available LC materials and the long wavelength of THz radiation. Furthermore, LC-based devices are typically controlled by externally applied electric fields, which necessitates the use of transparent electrodes [27, 28] not readily available in all regions of the spectrum, especially in THz [29]. The efficiency of LC-based devices in the THz regime can be substantially improved by the inclusion of metallic planar metamaterials (MMs). Such MMs are thin, metal films patterned on a sub-wavelength scale, enabling dramatic enhancement of diffraction-free light-matter interactions,

while maintaining a small device footprint (see e.g. [14, 30] and references therein). While thin layers of LCs integrated with MMs have been shown to be capable of effective modulation of THz radiation, their operation so far has been driven by externally applied electric fields and temperature [14, 30–38]. In our recent work we reported experimentally that such hybrid systems can also be controlled optically using the low-power THz radiation of a conventional THz-time domain spectrometer (TDS) [1]. The observed all-optical switching was attributed to a local in-plane reorientation of LC molecules induced by incident THz fields, which underwent resonant amplification and sub-wavelength concentration facilitated by the fabric of MMs. Here, we provide a comprehensive theoretical analysis of the proposed mechanism based on an analytical model of in-plane LC switching. We then confirm that engaging orientational optical nonlinearity of LCs at typical THz-TDS intensities is achievable with metallic MMs.

2. Experimental demonstration of optical switching

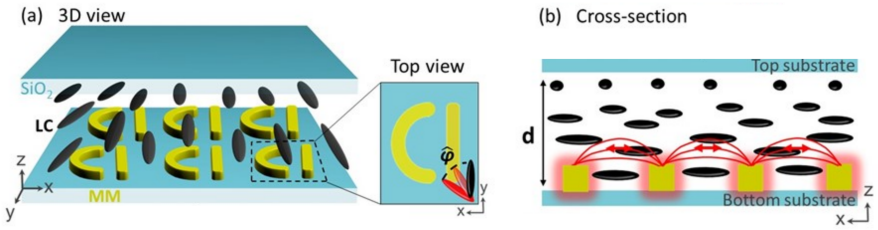

Fig. 1. (a) An artistic impression of a homogeneously aligned planar LC cell integrated with an array of D-shaped metallic resonators red(metamaterial). Inset shows schematically changes in the orientation of an LC molecule near a D-shaped resonator (and the associated twist angle, ϕ), driven by the near field. (b) Schematic representation of in-plane LC switching near the metamaterial induced by its resonantly enhanced near field (red arrows) in a homogeneously aligned hybrid LC cell.

For the sake of completeness and convenience to the reader, in this section we provide a brief account of our recent experimental study into LC optical switching using THz fields [1]. This study involved the characterisation of the transmission spectra of a 20µm thick LC optical cell hybridised with a metallic MM, using a conventional oscillator based THz-TDS setup in the 0.1-1.4 THz range of frequencies. The hybrid cell was filled with LC1825 and featured planar alignment set parallel to the straight sections of D-shaped MM resonators (metamolecules), as illustrated in Fig. 1(a). The measured spectrum shown with a black dashed line in Fig. 2(a) appeared blue-shifted with respect to the spectrum simulated for planar LC configuration (blue solid line) and displayed a smaller variation of transmission at the resonance. This surprising discrepancy was attributed to optically-induced local distortions of the initially planar alignment of the LC near the corners of the metamolecules ('hotspots'), where the re-orientation of LC molecules was driven by the resonantly amplified near field of the MMs (see Fig. 2(b)). To this end, the numerical model was modified to include the change in the refractive index of LC near the corners and in the gaps of D-shaped metallic resonators that would result from the re-orientation of LC molecules along the field lines. However, this would only occur when the direction of the local field deviated from the initial LC alignment by no more than $\pi/4$ (see inset to Fig. 2(a)). For other directions, (i.e., from $\pi/4$ to $\pi/2$) the local field was deemed too weak to ensure the complete re-orientation of LC molecules along its field lines. The transmission spectrum of the MM calculated using the modified numerical model is plotted in Fig. 2(a) with a red solid line and shows a good spectral overlap with the experimental data, thus, rendering

plausible our assumption that the deformation of planar LC alignment, ϕ, of up to $\pi/4$ was induced optically within the 'hotspots'. From the numerical model we also found that the overall local-field enhancement attainable with the MM was likely to exceed 200 [1], which suggested that in our case the orientational optical nonlinearity of LC might be engaged even with a low-power THz-TDS. In this work, we validate the above hypothesis using a simple analytical model of LC in-plane switching.

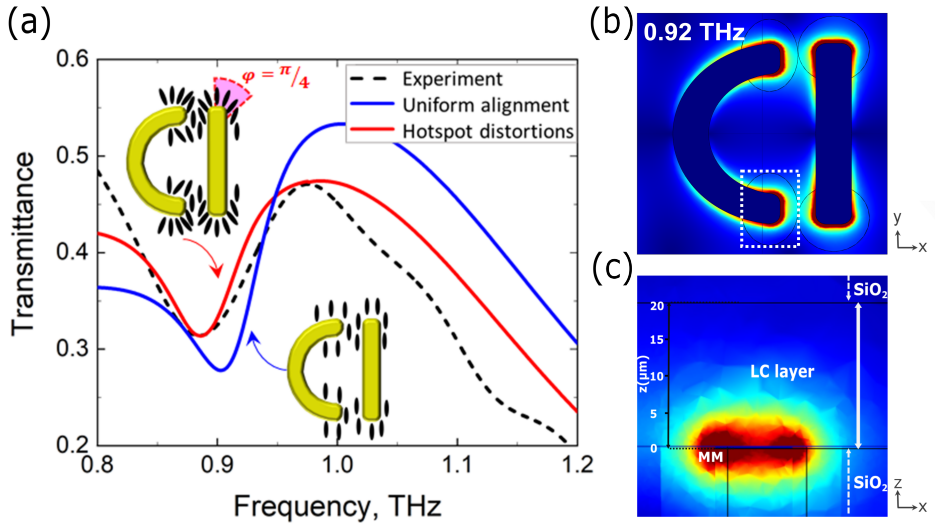

Fig. 2. (a) Transmission spectra of LC-loaded MM measured experimentally (black dash line) and modelled numerically in the cases when LC alignment is planar and uniform everywhere (blue solid curve) and distorted locally within 'hotspots' (red solid curve). Insets illustrate schematically the local alignment of LC molecules assumed in the two cases. Angle ϕ describes the twist deformation of LC in the 'hotspots' and has the maximum value of $\frac{\pi}{4}$. (b) Field map shows the variation of electric field induced in the plane of a metamolecule (xy-plane) at the resonance frequency of 0.92 THz. Electric field is strongest near the corners and in the gaps of the metamolecule. (c) Field map show the variation of the in-plane component of electric field induced in xz-plane near the corner of the metamolecule (marked by white rectangle in panel (b)).

3. Analytical model of LC optical switching

To estimate the strength of the THz field required to switch LCs in such hybrid cells we used a mathematical model previously developed for the analysis of the in-plane switching (IPS) of a nematic LCs [39]. Briefly, in the IPS model the electric field that re-orients LC molecules is produced by interdigital electrodes, which have an infinite length and are all arranged on the same plane (e.g., the surface of a substrate), forming two interlocking combs. It is assumed that every pair of neighbouring electrodes acts like a capacitor so that the electric field is homogeneous and aligned parallel to the substrate. In the OFF state, the LC molecules are oriented along the electrodes (see Fig. 3(a)). In the ON state, the electric field of the electrodes forces the LC molecules to orient along the field lines, i.e., orthogonal to the electrodes. Thus, IPS corresponds to $\pi/2$ 'in-plane' twist deformation of the LC (see Fig. 3(a)) [40,41]. Similarly, we assume that in our case the electric field induced at the corners of metamolecules, upon their illumination with a THz beam (ON state), drives the re-orientation of LC molecules within the 'hotspots'. This occurs in the plane of the MM, towards the direction of the field lines (see Fig. 1(b)). What

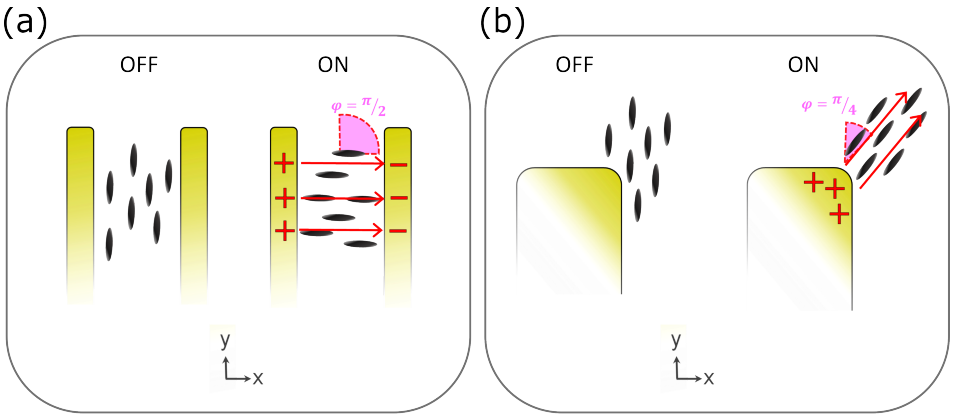

Fig. 3. (a) Schematically shown conventional in-plane switching mode of an LC cell (b) Schematically shown in-plane switching driven by the near field of a metamolecule, which models the re-alignment of LC in the area of the 'hotspot' where the initial misalignment between LC director and local field reaches $\pi/4$.

makes our case principally different from the conventional IPS model is that the electric field acting on the LC does not extend all the way across the cell, but is rather confined to a distance of few microns above the MM. More specifically, given that the local field decays exponentially within the hotspots, which is supported by the result of our simulation (see Fig. 2(c)), the spatial extent of the electric field is capped by $z_c = 2.9\mu m$, as given by e^{-1} falloff of the electric field strength. Thus, we use the IPS model approach locally, in close vicinity to the metamolecules, where the electric field is further assumed to be uniform and aligned parallel to the substrate. Another principle difference with the conventional IPS is that the twist deformation of LC, ϕ, in the areas featuring complete in-plane switching does not exceed $\pi/4$, as illustrated in Fig. 3(b). This fact was established earlier in [1] and, as we will show below, it lifts the restriction on the minimal strength of the electric field (i.e., voltage threshold) that can drive in-plane re-orientation of LC molecules and the resulting orientational optical nonlinearity of LC in the THz regime.

Following [39], we start with the free energy functional $F(\phi)$ of the twist deformation for the layer of LC subjected to the local electric field ($0 \le z \le z_c$), which has the form

$$F(\phi) = \frac{1}{2}\int_0^{z_c}\left(K_2\left(\frac{d\phi}{dz}\right)^2 - \epsilon_0\,|\Delta\epsilon|\,E^2\sin^2\phi\right)dz \tag{1}$$

where K_2 is the elastic constant of the twist deformation, ϕ is the twist angle in the xy-plane, $\Delta\epsilon$ denotes the dielectric anisotropy of LC, and E is the strength of the in-plane component of the local electric field. To further simplify the analysis, E is taken to be constant with the value given by the strength of the local field averaged across $0 \le z \le z_c$. To minimize the functional Eq. (1), ϕ must satisfy the following Euler-Lagrange equation.

$$K_2\frac{d^2\phi}{dz^2} + \epsilon_0\,|\Delta\epsilon|\,E^2\sin\phi\cos\phi = 0 \tag{2}$$

In the IPS model ϕ is defined as the angle between LC director and the direction orthogonal to the electric field lines and, hence, due to the initially planar alignment, LCs in the hotspots appear twisted with respect to the local field lines with ϕ being equal to or exceeding $\pi/4$ [1]. Thus, for those sectors of the hotspots that permit the largest optically-induced twist deformation the following substitution can be made: $\phi = \phi + \pi/4$, where ϕ now describes the deformation relative to the initial twist. As a result, Eq. (2) transforms into

$$K_2 \frac{d^2\phi}{dz^2} + \frac{\epsilon_0 |\Delta\epsilon| E^2}{2} \cos 2\phi = 0 \tag{3}$$

We proceed by solving Eq. (3) first under the assumption that the relative twist deformation is small, i.e., $\phi \to 0$. To find the solution we apply the following boundary conditions: $\phi = 0$ at $z = 0$ (corresponds to strong LC anchoring imposed on the MM side of the cell by rubbed polyimide) and $\frac{d\phi(z)}{dz} = 0$ at $z = z_c$, which stems from the transversality condition and effectively defines z_c as a 'free' boundary. In this case we arrive at the following solution

$$\phi(z) = \frac{\epsilon_0 |\Delta\epsilon| E^2}{4K_2}(2z_c - z)z \tag{4}$$

Evidently, Eq. (4) yields a non-zero ϕ for any $E \geq 0$, which indicates that in-plane reorientation of LC molecules within the hotspots starts with no threshold on the strength of the local electric field. This is in stark contrast to the conventional IPS mode, which manifests itself as a Fréedericksz transition and typically cannot be engaged with electric fields weaker than $1.05V/cm$ [39].

Next, we aim to find an analytical solution of Eq. (3), which will be valid in the limit of large relative twist angles, i.e., $\phi \to \pi/4$. To this end we linearise Eq. (3) by replacing $\cos 2\phi$ in the second term with its linear approximation at $\phi = \pi/4$. Here we have chosen the linear function that is tangential to $\cos 2\phi$ at $\phi = \pi/4$ (black dashed line Fig. 4(a)).

To this end, we use the approximation

$$\cos 2\phi \approx \pi/2 - 2\phi \tag{5}$$

which turns the initially nonlinear differential Eq. (3) into

$$K_2 \frac{d^2\phi}{dz^2} - \epsilon_0 |\Delta\epsilon| E^2 \phi + \epsilon_0 |\Delta\epsilon| E^2 \frac{\pi}{4} = 0 \tag{6}$$

Eq. (6) can now be solved analytically and its solution is given by

$$\phi(z, E) = \frac{\pi}{4} + k_1 \exp\left(-\sqrt{\frac{\epsilon_0 |\Delta\epsilon|}{K_2}} Ez\right) + k_2 \exp\left(\sqrt{\frac{\epsilon_0 |\Delta\epsilon|}{K_2}} Ez\right) \tag{7}$$

To determine k_1 and k_2, we use the same boundary conditions as above, namely $\phi(0) = \frac{d\phi(z_c)}{dz} = 0$. The derived expressions for k_1 and k_2 are

$$k_1 = -\left(\frac{\pi}{4} + k_2\right) \tag{8}$$

$$k_2 = -\frac{\pi \exp\left(-\sqrt{\frac{\epsilon_0|\Delta\epsilon|}{K_2}} Ez_c\right)}{8\left(\cosh\left(\sqrt{\frac{\epsilon_0|\Delta\epsilon|}{K_2}} Ez_c\right)\right)} \tag{9}$$

The constants in Eq. (7), (8) and (9) for LC1825 are taken from [42] (see table 1).

Constants	Values
ϵ_0	$8.85 \times 10^{-12}[N/V^2]$
$\Delta\epsilon$	17
K_2	$7.4 \times 10^{-12}[N]$

Table 1. Specifications of LC1825 [42]

4. Discussion

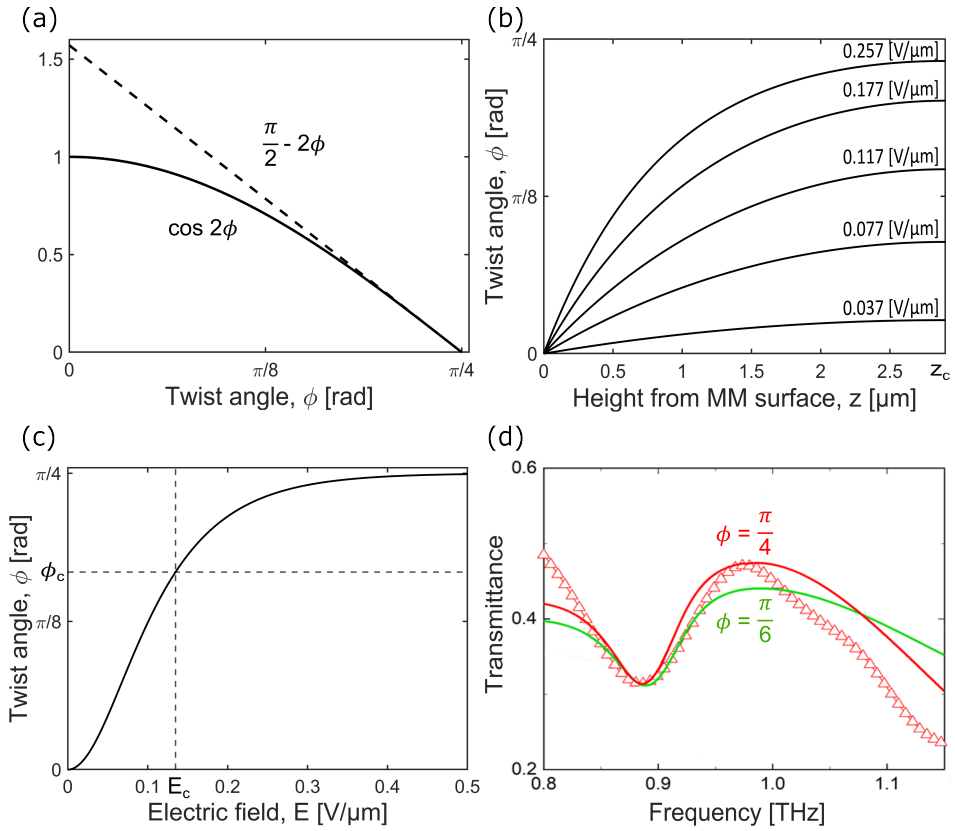

Fig. 4. (a) The linear approximation of $\cos 2\phi$ (solid line) approximated using $\frac{\pi}{2} - 2\phi$ (dashed line). (b) The change of twist angle, ϕ, within LC layer ($0 \geq z \geq z_c$), for different E-field values using the $\frac{\pi}{2} - 2\phi$ approximation. (c) The maximal twist angle, ϕ, achieved at $z = z_c$ as a function of the local electric-field strength, E. (d) Simulated results of the transmission spectra for hybrid LC cells at different angular limits of reorientation around MM 'hotspots' (solid lines), with experimental results (open triangles).

Figure 4(b) shows how the twist angle varies within a 2.9 μm thick layer of LC above the MM, as calculated using Eq. (7) for different values of the local electric-field strength. Evidently, the twist deformation increases monotonously away from the MM and saturates on approaching z_c. Note that while in-plane switching in our case features no voltage threshold, it formally remains incomplete since the analytical solution approaches $\pi/4$ asymptotically. This is best illustrated

by Fig. 4(c), where we plot the maximal twist angle (achieved at $z = z_c$) as a function of the local electric-field strength. Such behavior is underpinned by the dependence of the electrically induced LC torque on the twist angle. The torque in our case is proportional to $\cos 2\phi$ and, therefore, decreases with increasing ϕ, vanishing completely for LC molecules aligned parallel to the electric field (i.e., when $\phi = \pi/4$). In practice, however, the switching of LC within the hotspots does not have to be complete, as the dielectric permittivity of LC 'sensed' there by the local electric field is proportional to $\cos \Delta\phi$, where $\Delta\phi = \pi/4 - \phi$. If $\Delta\phi << 1$ the deviation of dielectric permittivity from the maximum value will be proportional to $\Delta\phi^2$ and, hence, appear insignificant.

Since the solution Eq. (7) is valid for $\phi \rightarrow \pi/4$, where the dependence on the local-field strength resembles a saturating exponential function (Fig. 4(c)), we take $\Delta\phi = \pi/4$e. It corresponds to a twist angle of $\pi/6$, which we regard as the 'characteristic' twist angle, ϕ_c. It defines $[0, \pi/6]$ as the range of LC twist deformations beyond which a significant change in the optical response of LC-loaded MM no longer occur, as also confirmed by our rigorous numerical modeling (see Fig. 4(d)). Hence, the characteristic twist angle can be used to determine the strength of local electric field, E_c, which would yield the level of optical switching comparable to that observed in the experiment [1]. Applying ϕ_c to the dependence plotted in Fig. 4(c) gives $E_c \approx 0.13V/\mu m$.

In the final part of our analysis we compare the typical strength of electric fields generated by a THz-TDS system with the strength of incident electric field required to seed the observed nonlinearity. To estimate the latter, we recall that local electric field decays exponentially away from the surface of the MM with e^{-1} falloff at 2.9 μm, while E_c in our analysis corresponds to the average value of the local-field strength. Hence, the electric field produced in the plane of the MM is a factor of 3 stronger than E_c. Since the field-enhancement factor characteristic of D-shaped metamolecules exceeds 200 [1], the required strength of electric field in an incident terahertz beam can be less than $3E_c/200 \approx 20V/cm$. Given that in conventional THz-TDS setups the electric field peered by THz detectors has the strength in the range from 10 to 100 V/cm [43], we conclude that the orientational optical nonlinearity of LCs can be readily engaged at THz frequencies with the help of purposely designed metallic MMs (at least, at the modest level observed in [1]). Also, we envisage that further optimisation of MM designs and the use of stronger sources of THz radiation will allow one to maximise the extent of LC all-optical switching in hybrid cells by enabling complete re-orientation of LC molecules even in those areas of the hotspots, where the initial misalignment between LC director and local field exceeds $\pi/4$. Among potential candidates for the THz sources that would be required, we have identified quantum cascade laser systems, which can achieve powers on the order of microwatts and up to milliwatts [44].

5. Conclusion

In this work, we analysed the nonlinear optical response of a liquid crystal cell hybridised with a metallic metamaterial and, in particular, a prominent shift of the metamaterial resonance frequency observed recently using a conventional oscillator-based terahertz time domain spectrometer [1]. We show that a local field enhancement exceeding a factor of 200 characteristic of the MM allows engaging nonlinear effects, despite the relatively low intensity radiation used. Indeed, a simple analytical model based on the in-plane switching mode of an liquid crystal cell confirms that the re-orientataion of liquid crystal near the metamaterial is a thresholdless process and incident terahertz electric field of as low as $\approx 20V/cm$ is strong enough to ensure the level of all-optical liquid crystal switching observed in the experiment. Our study paves a way towards systematic investigation of nonlinear optical effects in metamaterial-enhanced liquid crystal devices using conventional THz-TDS systems, with prospects for the development of low-power terahertz all-optical switches, spatial light modulators and image processors.

6. Corresponding author

7. Funding

8. Acknowledgments

n/a

9. Disclosures

The authors declare no conflicts of interest.

10. Data Availability Statement

??

11. Supplemental document

??

References

1. E. Perivolari, V. A. Fedotov, J. Parka, M. Kaczmarek, and V. Apostolopoulos, "Anomalous resonance frequency shift in liquid crystal-loaded thz metamaterials," Nanophotonics **11**, 2341–2348 (2022).
2. J. Y. Lu, L. J. Chen, T. F. Kao, H. H. Chang, H. W. Chen, A. S. Liu, Y. C. Chen, R. B. Wu, W. S. Liu, J. I. Chyi, and C. K. Sun, "Terahertz microchip for illicit drug detection," IEEE Photonics Technol. Lett. **18**, 2254–2256 (2006).
3. S. Al Tahhan and H. Aljobouri, "Sensing of illegal drugs by using photonic crystal fiber in terahertz regime," J. Opt. Commun. **-1** (2020).
4. E. Mavrona, U. Chodorow, M. E. Barnes, J. Parka, N. Palka, S. Saitzek, J. F. Blach, V. Apostolopoulos, and M. Kaczmarek, "Refractive indices and birefringence of hybrid liquid crystal - nanoparticles composite materials in the terahertz region," AIP Adv. **5** (2015).
5. B. Ning, Z. Chen, W. Chen, and L. Li, "Improving security of thz communication with intelligent reflecting surface," (Institute of Electrical and Electronics Engineers Inc., 2019).
6. J. F. Federici, B. Schulkin, F. Huang, D. Gary, R. Barat, F. Oliveira, and D. Zimdars, "Thz imaging and sensing for security applications - explosives, weapons and drugs," Semicond. Sci. Technol. **20** (2005).
7. P. Sharma, C. Liu, C. Ming, X. Wang, R. M. Woodward, B. E. Cole, V. P. Wallace, R. J. Pye, D. D. Arnone, E. H. Linfield, and M. Pepper, "Terahertz pulse imaging in reflection geometry of human skin cancer and skin tissue," (2002).
8. K. KrishneGowda, P. Rodriguez-Vazquez, L. Lopacinski, U. R. Pfeiffer, E. Grass, and R. Kraemer, "Thz transmission experiments – a data rate of 80 gbps was demonstrated using kasami codes," in *2021 IEEE International Conference on Microwaves, Antennas, Communications and Electronic Systems (COMCAS),* (2021), pp. 163–168.
9. L. D. Sio, G. Klein, S. Serak, N. Tabiryan, A. Cunningham, C. M. Tone, F. Ciuchi, T. Bürgi, C. Umeton, and T. Bunning, "All-optical control of localized plasmonic resonance realized by photoalignment of liquid crystals," J. Mater. Chem. C **1**, 7483–7487 (2013).
10. H.-K. Lee, A. Kanazawa, T. Shiono, T. Ikeda, T. Fujisawa, M. Aizawa, and B. Lee, "All-optically controllable polymer/liquid crystal composite films containing the azobenzene liquid crystal," (1998).
11. E. Perivolari, J. R. Gill, N. Podoliak, V. Apostolopoulos, T. J. Sluckin, G. D'Alessandro, and M. Kaczmarek, "Optically controlled bistable waveplates," J. Mol. Liq. **267**, 484–489 (2018).
12. L. D. Sio, E. Ouskova, P. Lloyd, R. Vergara, N. Tabiryan, and T. J. Bunning, "Light-addressable liquid crystal polymer dispersed liquid crystal," Opt. Mater. Express **7**, 1581 (2017).
13. C. M. Watts, D. Shrekenhamer, J. Montoya, G. Lipworth, J. Hunt, T. Sleasman, S. Krishna, D. R. Smith, and W. J. Padilla, "Terahertz compressive imaging with metamaterial spatial light modulators," Nat. Photonics **8**, 605–609 (2014).
14. O. Buchnev, N. Podoliak, K. Kaltenecker, M. Walther, and V. A. Fedotov, "Metasurface-based optical liquid crystal cell as an ultrathin spatial phase modulator for thz applications," ACS Photonics **7**, 3199–3206 (2020).
15. P. Weis, J. L. Garcia-Pomar, M. Höh, B. Reinhard, A. Brodyanski, and M. Rahm, "Spectrally wide-band terahertz wave modulator based on optically tuned graphene," ACS Nano **6**, 9118–9124 (2012).
16. C. C. Li, H. Y. Tseng, C. W. Chen, C. T. Wang, H. C. Jau, Y. C. Wu, W. H. Hsu, and T. H. Lin, "Versatile energy-saving smart glass based on tristable cholesteric liquid crystals," ACS Appl. Energy Mater. **3**, 7601–7609 (2020).
17. J. R. Talukder, H.-Y. Lin, and S.-T. Wu, "Photo- and electrical-responsive liquid crystal smart dimmer for augmented reality displays," Opt. Express **27**, 18169 (2019).
18. H. H. Khaligh, K. Liew, Y. Han, N. M. Abukhdeir, and I. A. Goldthorpe, "Silver nanowire transparent electrodes for liquid crystal-based smart windows," Sol. Energy Mater. Sol. Cells **132**, 337–341 (2015).

19. S. W. Oh, S. H. Kim, J. M. Baek, and T. H. Yoon, "Optical and thermal switching of liquid crystals for self-shading windows," Adv. Sustain. Syst. **2** (2018).
20. M. Bosch, M. R. Shcherbakov, K. Won, H. S. Lee, Y. Kim, and G. Shvets, "Electrically actuated varifocal lens based on liquid-crystal-embedded dielectric metasurfaces," Nano Lett. **21**, 3849–3856 (2021).
21. F. Gou, F. Peng, Q. Ru, Y.-H. Lee, H. Chen, Z. He, T. Zhan, K. L. Vodopyanov, and S.-T. Wu, "Mid-wave infrared beam steering based on high-efficiency liquid crystal diffractive waveplates," Opt. Express **25**, 22404 (2017).
22. J. Kobashi, H. Yoshida, and M. Ozaki, "Planar optics with patterned chiral liquid crystals," Nat. Photonics **10**, 389–392 (2016).
23. H. Yoshida and J. Kobashi, "Flat optics with cholesteric and blue phase liquid crystals," Liq. Cryst. **43**, 1909–1919 (2016).
24. N. Behabtu, J. R. Lomeda, M. J. Green, A. L. Higginbotham, A. Sinitskii, D. V. Kosynkin, D. Tsentalovich, A. N. G. Parra-Vasquez, J. Schmidt, E. Kesselman, Y. Cohen, Y. Talmon, J. M. Tour, and M. Pasquali, "Spontaneous high-concentration dispersions and liquid crystals of graphene," Nat. Nanotechnol. **5**, 406–411 (2010).
25. R. K. Gupta and A. A. Sudhakar, "Perylene-based liquid crystals as materials for organic electronics applications," Langmuir **35**, 2455–2479 (2019).
26. Y. Liu, Z. Xu, W. Gao, Z. Cheng, and C. Gao, "Graphene and other 2d colloids: Liquid crystals and macroscopic fibers," Adv. Mater. **29** (2017).
27. X. W. Lin, J. B. Wu, W. Hu, Z. G. Zheng, Z. J. Wu, G. Zhu, F. Xu, B. B. Jin, and Y. Q. Lu, "Self-polarizing terahertz liquid crystal phase shifter," AIP Adv. **1** (2011).
28. H. Y. Wu, C. F. Hsieh, T. T. Tang, R. P. Pan, and C. L. Pan, "Electrically tunable room-temperature 2 liquid crystal terahertz phase shifter," IEEE Photonics Technol. Lett. **18**, 1488–1490 (2006).
29. C. W. Chen, Y. C. Lin, C. H. Chang, P. Yu, J. M. Shieh, and C. L. Pan, "Frequency-dependent complex conductivities and dielectric responses of indium tin oxide thin films from the visible to the far-infrared," IEEE J. Quantum Electron. **46**, 1746–1754 (2010).
30. O. Buchnev, J. Wallauer, M. Walther, M. Kaczmarek, N. I. Zheludev, and V. A. Fedotov, "Controlling intensity and phase of terahertz radiation with an optically thin liquid crystal-loaded metamaterial," Appl. Phys. Lett. **103** (2013).
31. R. Wang, L. Li, J. Liu, F. Yan, F. Tian, H. Tian, J. Zhang, and W. Sun, "Triple-band tunable perfect terahertz metamaterial absorber with liquid crystal," Opt. Express **25**, 32280 (2017).
32. N. Chikhi, M. Lisitskiy, G. Papari, V. Tkachenko, and A. Andreone, "A hybrid tunable thz metadevice using a high birefringence liquid crystal," Sci. Reports **6** (2016).
33. L. Yang, F. Fan, M. Chen, X. Zhang, and S. J. Chang, "Active terahertz metamaterials based on liquid-crystal induced transparency and absorption," Opt. Commun. **382**, 42–48 (2017).
34. X. Li, N. Tan, M. Pivnenko, J. Sibik, J. A. Zeitler, and D. Chu, "High-birefringence nematic liquid crystal for broadband thz applications," Liq. Cryst. **43**, 955–962 (2016).
35. J. Wang, H. Tian, Y. Wang, X. Li, Y. Cao, L. Li, J. Liu, and Z. Zhou, "Liquid crystal terahertz modulator with plasmon-induced transparency metamaterial," Opt. Express **26**, 5769 (2018).
36. J. Yang, P. Wang, T. Shi, S. Gao, H. Lu, Z. Yin, W. Lai, and G. Deng, "Electrically tunable liquid crystal terahertz device based on double-layer plasmonic metamaterial," Opt. Express **27**, 27039 (2019).
37. S. Savo, D. Shrekenhamer, and W. J. Padilla, "Liquid crystal metamaterial absorber spatial light modulator for thz applications," Adv. Opt. Mater. **2**, 275–279 (2014).
38. Q. Zhao, L. Kang, B. Du, B. Li, J. Zhou, H. Tang, X. Liang, and B. Zhang, "Electrically tunable negative permeability metamaterials based on nematic liquid crystals," Appl. Phys. Lett. **90** (2007).
39. M. Oh-E and K. Kondo, "The in-plane switching of homogeneously aligned nematic liquid crystals," Liq. Cryst. **22**, 379–390 (1997).
40. R. A. Soref, "Field effects in nematic liquid crystals obtained with interdigital electrodes," J. Appl. Phys. **45**, 5466–5468 (1974).
41. M. Oh-E and K. Kondo, "Electro-optical characteristics and switching behavior of the in-plane switching mode," Appl. Phys. Lett. **67**, 3895 (1995).
42. U. Chodorow, J. Parka, K. Garbat, N. Paka, and K. Czupryński, "Spectral investigation of nematic liquid crystals with high optical anisotropy at thz frequency range," (2012), pp. 337–344.
43. P. U. Jepsen, R. H. Jacobsen, and S. R. Keiding, "Generation and detection of terahertz pulses from biased semiconductor antennas," (1996).
44. P. Dean, A. Valavanis, J. Keeley, K. Bertling, Y. L. Lim, R. Alhathlool, A. D. Burnett, L. H. Li, S. P. Khanna, D. Indjin, T. Taimre, A. D. Rakić, E. H. Linfield, and A. G. Davies, "Terahertz imaging using quantum cascade lasers - a review of systems and applications," J. Phys. D: Appl. Phys. **47** (2014).